New Multidimensional Visualization Technique for Limit-State Surfaces in Nonlinear Finite-Element Reliability Analysis

Michele Barbato, A.M.ASCE[1]; Quan Gu, A.M.ASCE[2]; and Joel P. Conte, M.ASCE[3]

Abstract: Structural reliability problems involving the use of advanced finite-element models of real-world structures are usually defined by limit-states expressed as functions (referred to as limit-state functions) of basic random variables used to characterize the pertinent sources of uncertainty. These limit-state functions define hyper-surfaces (referred to as limit-state surfaces) in the high-dimensional spaces of the basic random variables. The hyper-surface topology is of paramount interest, particularly in the failure domain regions with highest probability density. In fact, classical asymptotic reliability methods, such as the first- and second-order reliability method (FORM and SORM), are based on geometric approximations of the limit-state surfaces near the so-called design point(s) (DP). This paper presents a new efficient tool, the multidimensional visualization in the principal planes (MVPP) method, to study the topology of high-dimensional nonlinear limit-state surfaces (LSSs) near their DPs. The MVPP method allows the visualization, in particularly meaningful two-dimensional subspaces denoted as principal planes, of actual high-dimensional nonlinear limit-state surfaces that arise in both time-invariant and time-variant (mean out-crossing rate computation) structural reliability problems. The MVPP method provides, at a computational cost comparable with SORM, valuable insight into the suitability of FORM/SORM approximations of the failure probability for various reliability problems. Several application examples are presented to illustrate the developed MVPP methodology and the value of the information provided by visualization of the LSS.

DOI: 10.1061/(ASCE)EM.1943-7889.0000183

CE Database subject headings: Finite element method; Structural reliability; Limit states; Imaging techniques.

Author keywords: Nonlinear finite-element method; Structural reliability analysis; Limit-state surface; Hyper-surface topology; Multidimensional visualization.

Introduction

The field of structural reliability analysis has seen significant advances in the last two decades (Ditlevsen and Madsen 1996; Schueller et al. 2004). Analytical and numerical methodologies have been developed for the probabilistic analysis of real structures characterized by nonlinear behavior and material/geometric uncertainties, and subjected to stochastic loading. Reliability analysis methods have been successfully applied to problems encountered in civil engineering, which in the deterministic realm are typically analyzed through the finite-element (FE) method (Der Kiureghian and Ke 1988).

In general, a structural reliability problem requires computing a probability of failure, P_f, corresponding to some limit-state (or damage-state) function(s) (LSFs) when the loading(s) and/or structural properties and/or parameters in the LSFs are uncertain quantities modeled as random variables. These LSFs define a failure domain (LSF<0), a safe domain (LSF>0), and a limit-state surface (LSS) (LSF$=0$). Thus, P_f is the probability content of the failure domain (Ditlevsen and Madsen 1996). Among the reliability analysis methods available, asymptotic (semi-analytical) methods [first- and second-order reliability methods (FORM and SORM)] (Breitung 1984; Der Kiureghian et al. 1987) and some sampling techniques (Melchers 1989; Au et al. 1999; Au and Beck 2001b) are characterized by the crucial step of finding the design points (DPs), defined as the most likely failure points in the standard normal space. Asymptotic methods can provide reliability analysis results with a relatively small number of LSF evaluations (often of the order of 10~100 for FORM analysis, corresponding to the number of iterations required to find the DP) and with a computational effort only weakly dependent on the magnitude of the failure probability. It is noteworthy that, while the number of LSF evaluations is practically independent of the number of random variables, the computational cost of each iteration in the DP search increases with the number of random variables. Furthermore, these methods provide important information (e.g., reliability sensitivity measures) as a by-product of the DP search (Hohenbichler and Rackwitz 1986). On the other hand,

[1]Assistant Professor, Dept. of Civil and Environmental Engineering, Louisiana State Univ. and A&M College, 3531 Patrick F. Taylor Hall, Nicholson Extension, Baton Rouge, LA 70803. E-mail: mbarbato@lsu.edu

[2]Associate Professor, School of Architecture and Civil Engineering, Xiamen Univ., Xiamen, Fujian, People's Republic of China; formerly, Postdoctoral Researcher, Dept. of Structural Engineering, Univ. of California at San Diego, 9500 Gilman Dr., La Jolla, CA 92093-0085 (corresponding author). E-mail: quan.gu.ucsd@gmail.com

[3]Professor, Dept. of Structural Engineering, Univ. of California at San Diego, 9500 Gilman Dr., La Jolla, CA 92093-0085. E-mail: jpconte@ucsd.edu

Note. This manuscript was submitted on November 24, 2009; approved on April 19, 2010; published online on April 21, 2010. Discussion period open until April 1, 2011; separate discussions must be submitted for individual papers. This paper is part of the ***Journal of Engineering Mechanics***, Vol. 136, No. 11, November 1, 2010. ©ASCE, ISSN 0733-9399/2010/11-1390–1400/$25.00.

convergence of the DP search iterative process can be numerically very challenging, and the nonlinearities in the LSS can cause inaccuracies in the FORM/SORM failure probability estimates. Other reliability analysis methods, e.g., subset simulation (Au and Beck 2001a, 2003) and importance sampling with sampling distribution not centered at the DP(s) (Bucher 1988; Ang et al. 1992), do not use the concept of DP. In general, the computational cost of these methods increases for decreasing failure probability. Thus, for reliability problems with very low failure probabilities (i.e., $10^{-3} \sim 10^{-7}$ typical of civil structures), these methods could require a prohibitively large number of simulations.

The geometric properties of LSSs encountered in FE reliability analysis problems are of great research interest. FORM/SORM analyses are based on geometric approximations of the LSS at the DP (Der Kiureghian 2000). Importance sampling methods can be extremely efficient when information about the LSS geometry is used (Au and Beck 2001b). Knowledge of the LSS topology for a given FE reliability analysis problem is particularly valuable in: (1) gaining physical and geometrical insight into the structural reliability problem at hand (e.g., singly versus multiply connected failure domain); (2) understanding the reasons behind potential difficulties encountered in the DP search (e.g., nonsmoothness of the LSS); (3) developing more robust and more efficient DP search algorithms exploiting the physical and geometrical insight gained; (4) identifying the sources of inaccuracy of the FORM/SORM approximations for time-invariant and time-variant (mean out-crossing rate computation) FE reliability analysis problems (Barbato 2007); and (5) pointing to new more efficient and more accurate computational methods for evaluating the probability content of failure domains typically encountered in FE structural reliability analysis.

Nevertheless, only scarce research has been devoted to gain insight into the geometric properties of nonlinear LSSs typically arising in FE reliability analysis of nonlinear structural models subjected to random loading (Der Kiureghian 2000). This is likely due to the fact that the study of the topology of LSSs is a challenging task involving visualization of nonlinear hypersurfaces in high-dimensional spaces (i.e., physical space or standard normal space defined by numerous random variables related to loading, geometric and material parameters). Indeed, only limited tools (Haukaas and Der Kiureghian 2004) are available to visualize, in nonspecialized two- or three-dimensional subspaces of high-dimensional spaces, LSFs and LSSs corresponding to FE reliability analysis problems. These non-specialized subspaces are defined by sets of two or three arbitrary axes of the standard normal space in which the reliability problem is cast. In this study, a new method is developed for the visualization, in the neighborhood of the DP, of LSSs in high-dimensional spaces for both time-invariant and time-variant FE structural reliability analysis. This new approach is referred to herein as the multidimensional visualization in the principal planes (MVPP) method. The MVPP method provides extremely valuable information on the geometric properties of the actual LSSs and how they affect the accuracy of the estimated failure probability for FE structural reliability problems in high-dimensional spaces of random variables. This geometric information is obtained at a limited computational cost, which is only weakly dependent on the number of random variables. To the writers' knowledge, the MVPP method provides a first and unique practical visualization tool to extract crucial topological information on nonlinear high-dimensional LSSs in FE structural reliability analysis. Thus, the MVPP results about the actual geometry of the LSSs are significantly different from other qualitative (conceptual) depictions of LSSs, which have been commonly used for descriptive purposes in the literature on structural reliability analysis (Schueller 2008).

MVPP Method

This paper presents the MVPP method to study the geometry of LSSs near their DPs in spaces with more than three dimensions in the context of structural reliability analysis. This method is especially useful for high-dimensional spaces, such as the ones defined by the large number of random variables typically encountered in FE reliability analysis. The basic idea behind the MVPP method is to visualize the LSS in the neighborhood of the DPs in two-dimensional subspaces (i.e., planes) of particular interest. These planes are referred to as the principal planes (PPs) and are defined as the planes of principal curvatures of the LSS at the DPs. The MVPP consists in finding the traces of the LSS in the PPs (i.e., the intersection curves between the LSS and the PPs), with the PPs ordered in decreasing magnitude of the LSS principal curvatures at the DP(s). In the case of an LSS with multiple DPs, the MVPP method can be applied repeatedly to visualize the LSS in the neighborhood of each DP. The MVPP method has been implemented and tested in two different computational frameworks, namely OpenSees (Mazzoni et al. 2007) and FedeasLab-FERUM (Haukaas 2001; Filippou and Constantinides 2004).

The MVPP method encompasses the following major steps: (1) search of the DPs; (2) determination of the PPs of interest; and (3) computation and visualization of the traces of the LSS in these PPs. Next, the three stages of the methodology are described in detail for time-invariant component reliability analysis. Then, the MVPP method is extended to time-variant component reliability problems. In the sequel, the boldface and lightface represent a vector/matrix and scalar value, respectively.

Step 1: Design Point Search

A component reliability analysis problem is defined by a single LSF $g = g(\boldsymbol{r}, \boldsymbol{\theta})$, where $\boldsymbol{r}$ = vector of response quantities of interest and $\boldsymbol{\theta}$ = vector of basic random variables. The LSF g is chosen such that $g \leq 0$ defines the failure domain/region. Thus, the time-invariant component reliability problem can be expressed mathematically as (Ditlevsen and Madsen 1996)

$$P_f = P[g(\boldsymbol{r}, \boldsymbol{\theta}) \leq 0] = \int_{g(\boldsymbol{r}, \boldsymbol{\theta}) \leq 0} f_{\Theta}(\boldsymbol{\theta}) d\boldsymbol{\theta} \tag{1}$$

where $f_{\Theta}(\boldsymbol{\theta})$ = joint probability density function (PDF) of all basic random variables $\boldsymbol{\theta}$.

A well-established methodology to solve the problem in Eq. (1) consists of converting it from the space of original/physical random variables $\boldsymbol{\theta}$ to the space of standard normal uncorrelated random variables $\boldsymbol{y}$ (referred to as the standard normal space). It can be shown that, provided the joint cumulative distribution function of random variables $\boldsymbol{\theta}$ is continuous and monotonically increasing as a function of each random variable, a one-to-one mapping between the physical space and the standard normal space can be found (Ditlevsen and Madsen 1996). With this change of variables, Eq. (1) is recast as

$$P_f = P[G(\mathbf{y}) \le 0] = \int_{G(\mathbf{y})\le 0} \phi_{\mathbf{Y}}(\mathbf{y})d\mathbf{y} \tag{2}$$

where $\phi_{\mathbf{Y}}(\mathbf{y})$=standard normal joint PDF and $G(\mathbf{y})$=LSF in the standard normal space. Solving the integral in Eq. (2) remains a formidable task, but this new form of P_f is suitable for approximate solutions taking advantage of the rotational symmetry of the standard normal joint PDF and its exponential decay in both the radial and tangential directions. An optimum point at which to approximate the LSS and evaluate the integral in Eq. (2) is the DP, which is defined as the point on the LSS nearest to the origin. The DP, $\mathbf{y}^*$, is found as solution of a nonlinear constrained optimization problem (Liu and Der Kiureghian 1991). The most effective techniques for finding the DP are gradient-based optimization algorithms (Gill et al. 1981; Liu and Der Kiureghian 1991) coupled with algorithms for accurate and efficient computation of the gradient, $\nabla_{\mathbf{y}}G$, of the constraint function $G(\mathbf{y})$ with respect to the standard normal variables $\mathbf{y}$. Using the chain rule of differentiation for multivariable functions and recognizing that $g = g(\mathbf{r}(\boldsymbol{\theta}), \boldsymbol{\theta})$, $\nabla_{\mathbf{y}}G$ is computed as

$$\nabla_{\mathbf{y}}G = (\nabla_{\mathbf{r}}g|_{\boldsymbol{\theta}} \cdot \nabla_{\boldsymbol{\theta}}\mathbf{r} + \nabla_{\boldsymbol{\theta}}g|_{\mathbf{r}}) \cdot \nabla_{\mathbf{y}}\boldsymbol{\theta} \tag{3}$$

where $\nabla_{\mathbf{r}}g|_{\boldsymbol{\theta}}$ and $\nabla_{\boldsymbol{\theta}}g|_{\mathbf{r}}$=gradients of LSF g with respect to its explicit dependency on quantities $\mathbf{r}$ and θ, respectively, which usually can be computed analytically; $\nabla_{\boldsymbol{\theta}}\mathbf{r}$=sensitivities of response variables $\mathbf{r}$ to parameters $\boldsymbol{\theta}$, $\nabla_{\mathbf{y}}\boldsymbol{\theta}$=gradient of the physical space parameters with respect to the standard normal space parameters (i.e., Jacobian matrix of the probability transformation from the $\mathbf{y}$-space to the $\boldsymbol{\theta}$-space), and the operator $\bullet|_x$ indicates that the quantity to which it is attached is computed keeping constant the value of the variable x. For probability distribution models defined analytically, the gradient $\nabla_{\mathbf{y}}\boldsymbol{\theta}$ can be derived analytically as well (Ditlevsen and Madsen 1996). For real-world problems, response simulation (computation of $\mathbf{r}$ for given $\boldsymbol{\theta}$) is usually performed using advanced, high-fidelity, mechanics-based nonlinear computational models based on the FE method. FE reliability analysis requires augmenting existing FE formulations for response-only calculation to compute the response sensitivities to parameters $\boldsymbol{\theta}$, $\nabla_{\boldsymbol{\theta}}\mathbf{r}$. An accurate and efficient method for FE response sensitivity analysis is the direct differentiation method (DDM) (Zhang and Der Kiureghian 1993; Kleiber et al. 1997; Conte et al. 2003, 2004; Haukaas and Der Kiureghian 2004; Barbato and Conte 2005, 2006; Zona et al. 2005, 2006; Barbato et al. 2007; Gu et al. 2009a,b).

The DP search, for FE reliability analysis involving large-scale nonlinear models of real-world structural systems, is itself a challenging task. Herein, the nonlinear optimization code SNOPT (Gill et al. 2002) is employed for the DP search (Gu 2008) in conjunction with DDM-based response sensitivities for evaluating the LSF gradient [Eq. (3)].

Step 2: Determination of the PPs of Interest

After finding the DP, a new reference system in the standard normal space is defined so that the nth axis (with n=number of random variables) is oriented in the direction defined by the DP vector $\mathbf{y}^*$ and the new origin coincides with the DP. A generic vector $\mathbf{y}'$ in the new reference system is obtained as $\mathbf{y}' = \mathbf{R}\cdot(\mathbf{y}-\mathbf{y}^*)$ where the rotation matrix $\mathbf{R}$ is defined such that $\mathbf{R}\cdot\mathbf{y}^* = [0 \ \cdots \ 0 \ \beta]^{\mathrm{T}}$, in which β=distance of the DP from the origin (i.e., FORM reliability index). The rotation matrix $\mathbf{R}$ can be determined using any suitable **QR** decomposition algorithm, e.g., classical and modified Gram-Schmidt orthonormalization (Stoer and Bulirsch 2002). Notice that $\mathbf{R}$ is uniquely defined when the employed **QR** algorithm is specified.

Each PP is defined by the DP vector $\mathbf{y}^*$ (nth axis of the transformed reference system) and one of the eigenvectors (referred to as principal directions) of the (normalized and reduced) Hessian matrix $\mathbf{A}$ defined as (Breitung 1984)

$$\mathbf{A} = \frac{\mathbf{H}_{\mathrm{red}}}{\|\nabla_{\mathbf{y}}G|_{\mathbf{y}=\mathbf{y}^*}\|} \tag{4}$$

in which $\mathbf{H}_{\mathrm{red}} = (n-1)\times(n-1)$ reduced Hessian computed at the DP in the transformed reference system, obtained by deleting the nth column and nth row from the $(n\times n)$ Hessian matrix of the LSF at the DP in the transformed reference system, i.e., $\mathbf{R}\cdot\mathbf{H}\cdot\mathbf{R}^{\mathrm{T}}$, where $\mathbf{H}=(n\times n)$ Hessian matrix of the LSF at the DP in the standard normal space, $\|\nabla_{\mathbf{y}}G|_{\mathbf{y}=\mathbf{y}^*}\|$=Euclidean norm of the gradient of the LSF at the DP in the standard normal space, and the operator $\bullet|_{x=\bar{x}}$ indicates that the quantity to which it is attached is evaluated at $x=\bar{x}$. Herein, the LSF is assumed to be twice differentiable in the neighborhood of the DP, thus ensuring existence of the Hessian matrix at the DP. A sufficient condition for this assumption to be satisfied is that, when using only uniaxial material models, all material constitutive models are continuously differentiable with respect to the material parameters, the loading function is continuous in time and continuously differentiable with respect to the loading parameters modeled as random variables, and (for reliability problems based on dynamic FE analysis) the time step used to integrate the equations of motion of the system is sufficiently small (Barbato and Conte 2006). The principal directions are sorted in decreasing order of magnitude (absolute value) of the corresponding eigenvalues which represent the principal curvatures. Only a limited number of principal directions are computed (using any algorithm for finding the eigenvalues/eigenvectors of a real-valued symmetric square matrix), thus defining a limited number of PPs in which the topological properties of the LSS are of interest. The number of principal directions of interest can be defined by setting a lower limit $|\beta\kappa|_{\min}$ to the adimensional (normalized) quantity $|\beta\kappa_i|$, where $\kappa_i = i$th principal eigenvalue ($i=1,\ldots,n-1$), below which visualization in the corresponding PP is not needed since the trace of the LSS in this PP is almost linear in the neighborhood of the DP.

In this study, the Hessian matrix $\mathbf{H}$ in the standard normal space [see Eq. (4)] is obtained by forward finite difference calculations applied to the DDM-based FE response sensitivities. The finite difference calculations can be performed either: (1) in the physical space to obtain the Hessian matrix $\mathbf{H}_{\boldsymbol{\theta}}$ which is then transformed to the Hessian matrix $\mathbf{H}$ in the standard normal space, or (2) in the standard normal space to obtain directly $\mathbf{H}$. It was observed that the second procedure is less prone to numerical difficulties and inaccuracies and is adopted herein. After selecting a perturbation value, Δy, for the standard normal random variables (e.g., $\Delta y = 10^{-3} \sim 10^{-5}$), the ith row of the Hessian matrix, $\mathbf{H}_i$, is approximated as

$$\mathbf{H}_i \cong \frac{1}{\Delta y}[\nabla_{\mathbf{y}}G|_{\mathbf{y}=\mathbf{y}^*+\Delta y\cdot\mathbf{e}_i} - \nabla_{\mathbf{y}}G|_{\mathbf{y}=\mathbf{y}^*}] \tag{5}$$

in which $\mathbf{e}_i = i$th axis unit vector, i.e., a column vector with the ith component equal to one and all other components equal to zero. The row vector $\nabla_{\mathbf{y}}G|_{\mathbf{y}=\mathbf{y}^*+\Delta y\cdot\mathbf{e}_i}$ in the equation is obtained by: (1) perturbing the DP vector in the standard normal space as $\mathbf{y}^{(i)} = \mathbf{y}^* + \Delta y\cdot\mathbf{e}_i$; (2) mapping $\mathbf{y}^{(i)}$ to the corresponding point $\boldsymbol{\theta}^{(i)}$ in the physical space; (3) computing the gradient $\nabla_{\boldsymbol{\theta}}g|_{\boldsymbol{\theta}=\boldsymbol{\theta}^{(i)}}$ in the physi-

cal space; and (4) transforming the obtained gradient back to the standard normal space, i.e., $\nabla_y G|_{y=y^*+\Delta y\cdot e_i} = \nabla_\theta g|_{\theta=\theta^{(i)}} \cdot \nabla_y \theta|_{y=y^*+\Delta y\cdot e_i}$.

The DDM-based forward finite difference method defined above is more efficient and accurate for computing the Hessian matrix $\boldsymbol{H}$ than the second-order central finite difference method applied directly to the LSF. Nevertheless, for detailed FE models of realistic structural systems characterized by a large number of uncertain model parameters, this approach for computing the Hessian matrix could still be computationally prohibitive. To significantly reduce the computational cost of the MVPP method, an existing algorithm (Der Kiureghian and De Stefano 1991) can also be used to obtain the principal directions in order of decreasing magnitude of the corresponding eigenvalues without computing the entire Hessian matrix $\boldsymbol{H}$.

Step 3: Visualization of Traces of LSS in PPs

Visualization of the traces of the LSS in the PPs of interest can be obtained using two methods: (1) computing the values of the LSF over a grid of points in the PP and obtaining the trace of the LSS in this PP as zero level curve of the discretely sampled surface so obtained, and (2) employing a standard zero-finding algorithm (for scalar functions of a single variable) to obtain points of the LSS trace as zero points of the LSF in the PP. These two methods will be referred to hereafter as the zero level curve method (ZLCM) and the zero-finding method (ZFM), respectively. In the ZFM, the zero-finding is performed in the PP local coordinate system with origin at the DP, x-axis defined by the corresponding principal direction in this PP, and y-axis defined by the DP direction. For each selected point x_p on the x-axis ($p=1,2,\ldots,n_{pt}$, with n_{pt}=user-defined number of points along the x-axis), the value of the LSF G along the y-axis depends only on the value of the coordinate y. A zero-finding algorithm is used to find the value y_p so that $G(y_p)=0$. The starting point for the zero-finding algorithm at each considered x_p can be taken on the x-axis (i.e., $y=0$). The ZFM is usually much more efficient than the ZLCM if a robust and efficient zero-finding algorithm (e.g., safeguarded secant or Newton's method, see Gill et al. 1981) is employed.

LSS visualization is performed only in the (usually small number of) PPs corresponding to the set of principal curvatures κ_i satisfying the condition $|\beta\kappa_i| \geq |\beta\kappa|_{\min}$. For increasing order of the PP (i.e., for decreasing absolute value of the corresponding principal curvature), the LSS trace in the neighborhood of the DP increasingly approaches a straight line coincident with the x-axis. Therefore, the MVPP method provides important information on the LSS topology near the DPs (e.g., nonlinearity, smoothness) and on the geometry of the failure domain (e.g., global/local shape, singly/multiply connected) by identifying a small number of most important two-dimensional subspaces (i.e., PPs) and thus by requiring only a limited number of FE simulations to visualize the LSS.

Extension of MVPP to Time-Variant Reliability Problems

In time-variant reliability problems, the objective is to compute the time-variant failure probability, $P_f(T)$, defined as the probability of occurrence of at least one out-crossing event in the failure domain over the time interval $[0, T]$. Classical approaches to solving time-variant reliability problems make use of estimates of the mean down-crossing rate of level zero of the LSF g, $\nu_g(t)$ (in short, mean outcrossing rate: MOCR). In time-variant reliability analysis, the LSF also depends on the time t and can be expressed, in general, as $g=g(\boldsymbol{r}(\boldsymbol{\theta},t),\boldsymbol{\theta},t)=g(\boldsymbol{\theta},t)$ in the original/physical space, or as $G=G(\boldsymbol{y},t)$ in the standard normal space. The mean out-crossing rate $\nu_g(t)$ is given in limit form as (Hagen and Tvedt 1991)

$$\nu_g(t) = \lim_{\delta t \to 0} \frac{P[(G_1 < 0) \cap (G_2 \leq 0)]}{\delta t} \tag{6}$$

where $G_1=-G(\boldsymbol{y},t)$ and $G_2=G(\boldsymbol{y},t+\delta t)$. The numerator in the right-hand side (r.h.s.) of Eq. (6) is the probability that the system is in the safe domain at time t and in the unsafe domain at time $t+\delta t$, where δt=small but finite interval of time. Thus, a numerical approximation of the MOCR can be obtained by taking a finite δt (sufficiently small to preclude the possibility of more than one out-crossing event in the time interval $(t, t+\delta t]$), evaluating the numerator in the r.h.s. of Eq. (6) and dividing it by δt. The evaluation of this numerator at a given instant of time t corresponds to solving a time-invariant parallel system reliability problem of two components with LSFs G_1 and G_2, respectively. Therefore, in the case of time-variant reliability problems, interest is on the visualization of the two LSSs $G_1=0$ (at time t) and $G_2=0$ (at time $t+\delta t$) and the domain between these two hyper-surfaces. Indeed, the probability content of this domain is the numerator in the r.h.s. of Eq. (6). In addition to visualizing the LSS $G_1=0$ as in time-invariant reliability analysis, the MVPP method for time-variant reliability analysis requires the additional step of visualizing the LSS $G_2=0$. After evaluating G_1 at a given point in the considered PP, the LSF G_2 at the same point can be computed at negligible computational cost (without any additional FE response simulation) as

$$G_2 = G(\boldsymbol{y}, t+\delta t) \cong G(\boldsymbol{y},t) + \frac{\partial G}{\partial t}\cdot \delta t = g(\boldsymbol{\theta},t) + \nabla_{\boldsymbol{r}} g|_{\boldsymbol{\theta}} \cdot \frac{\partial \boldsymbol{r}}{\partial t}\cdot \delta t \tag{7}$$

In the ZLCM, the LSF G_2 is evaluated directly using Eq. (7) on the same grid of points used for the LSF G_1. In the ZFM, points on the trace of the LSS $G_2=0$ in the PP of interest are obtained efficiently using information from the zero-finding iterations performed to obtain the corresponding points on the trace of the LSS $G_1=0$. This information consists of the coordinates of the point(s) where G_2 assumes the smallest positive and/or largest negative value(s) and the value(s) of G_2 at this (these) point(s) for each iteration sequence yielding a point on the trace of the LSS $G_1=0$.

Application Examples

First, the MVPP method is illustrated in a time-invariant component reliability problem defined by an analytical LSF. Then, two application examples of time-invariant and time-variant component reliability analysis related to two different nonlinear FE structural models are presented to demonstrate the capabilities of the proposed method and its utility. In each of these three application examples, the MVPP results are analyzed and used to gain insight into the accuracy or lack thereof of FORM/SORM approximations to the failure probability.

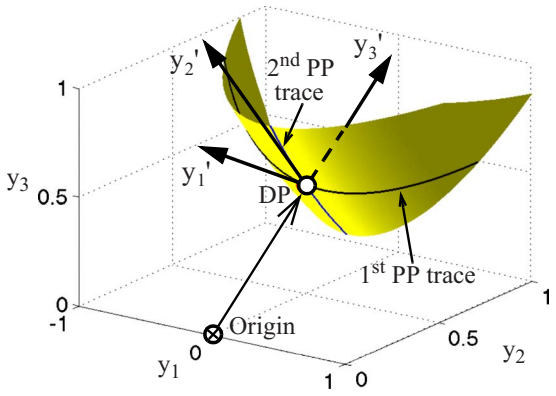

Fig. 1. Three-dimensional visualization of the analytical LSS in the standard normal space

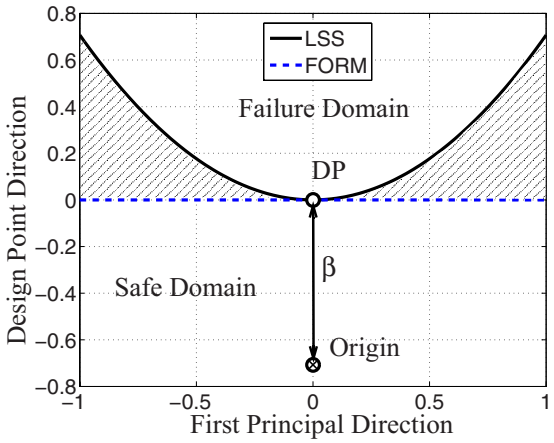

Fig. 2. MVPP for time-invariant reliability analysis with analytical LSF: visualization in the first PP (shaded area=difference between actual failure domain and its FORM approximation)

Time-Invariant Case: LSF Defined by an Analytical Function

The first application example consists of a time-invariant component reliability problem with an analytical LSF depending on three statistically independent standard normal variables y_i $(i=1,2,3)$. This simple case study is used here to clearly illustrate the MVPP method step by step. The analytical LSF considered is defined as

$$G(\boldsymbol{y}) = \frac{61}{80}y_1^2 + \frac{27}{160}(y_2^2+y_3^2) + \frac{19\sqrt{6}}{80}y_1(y_2-y_3) - \frac{19}{80}y_2y_3 - \frac{21}{20}(y_2+y_3) + \frac{41}{40} \tag{8}$$

Three-dimensional visualization of the LSS $G(\boldsymbol{y})=0$ is given in Fig. 1. The DP is located at $\boldsymbol{y}^*=[0\ 0.5\ 0.5]^T$ and the FORM reliability index assumes the value $\beta=\sqrt{2}/2$. The rotation matrix $\boldsymbol{R}$ is obtained via Gram-Schmidt orthonormalization and the LSF in the transformed reference system is given by

$$G(\boldsymbol{y}') = \frac{61}{80}y_1'^2 + \frac{23}{80}y_2'^2 + \frac{1}{20}y_3'^2 - \frac{19\sqrt{3}}{40}y_1'y_2' - \sqrt{2}y_3' \tag{9}$$

The norm of the gradient vector at the DP in the standard normal space is $\|\nabla_{\boldsymbol{y}}G|_{\boldsymbol{y}^*}\|=\sqrt{2}$ and the normalized and reduced Hessian matrix $\boldsymbol{A}$ at the DP in the transformed reference system is

$$\boldsymbol{A} = \frac{\sqrt{2}}{80}\begin{bmatrix} 61 & 19\sqrt{3} \\ 19\sqrt{3} & 23 \end{bmatrix} \tag{10}$$

The eigenvalues of matrix $\boldsymbol{A}$ are $\kappa_1=\sqrt{2}$ and $\kappa_2=\sqrt{2}/20$, with $|\beta\kappa_1|=1$ and $|\beta\kappa_2|=0.05$, respectively. Figs. 2 and 3 show the visualization using the MVPP method of the analytical LSS in the first PP and second PP, respectively. The traces of the LSS in the first and second PPs are obtained through the ZLCM using a grid of points in the considered PPs extending from -0.8 to $+0.8$ in the direction of the DP vector y^* and from -1.0 to $+1.0$ in the first and second principal directions. The LSF is evaluated at 41 grid points in each direction of the PPs, for a total of $n_{FE}=41^2-1=1,680$ function evaluations. Then, the two traces are obtained using the Matlab function "contour" (MathWorks 1997). The trace of the LSS in the first PP differs considerably from the straight line which corresponds to the FORM approximation. In the second PP, the parameter $|\beta\kappa_2|$ is small compared to $|\beta\kappa_1|$ and the trace of the LSS is very close to the straight line corresponding to the FORM approximation. In general, for decreasing value of $|\beta\kappa_i|$, the trace of the LSS in the ith PP near the DP gets closer to the straight line corresponding to the FORM approximation of the LSS. This observation justifies the choice of the PPs in which visualization of the LSS is of interest, based on the lower limit $|\beta\kappa|_{\min}$ for parameter $|\beta\kappa_i|$. Estimates of the failure probability, P_f, obtained by using several different computational reliability methods are: $P_{f,\mathrm{FORM}}=0.2398$ (FORM), $P_{f,\mathrm{SORM,B}}=0.1654$ (SORM based on Breitung's formula, Breitung 1984), $P_{f,\mathrm{SORM,HR}}=0.1533$ (SORM based on Hohenbichler-Rackwitz's formula, Hohenbichler and Rackwitz 1988), $P_{f,\mathrm{IS}}=0.1285$ (importance sampling with a coefficient of variation $\mathrm{COV}[P_{f,\mathrm{IS}}]=0.005$, taken as reference solution, obtained after 109,894 simulations). As expected from the visualization of the LSS obtained using the MVPP method, FORM provides only a poor approximation to the failure probability, while SORM provides significantly improved approximations of the failure probability. In this problem, the difference between the actual LSS and its FORM approximation in the first PP has a dominant effect, compared to the difference observed in the second PP, on the discrepancy between the actual failure probability and its FORM estimate. It is noteworthy that, in general, a positive principal curvature results in an overestima-

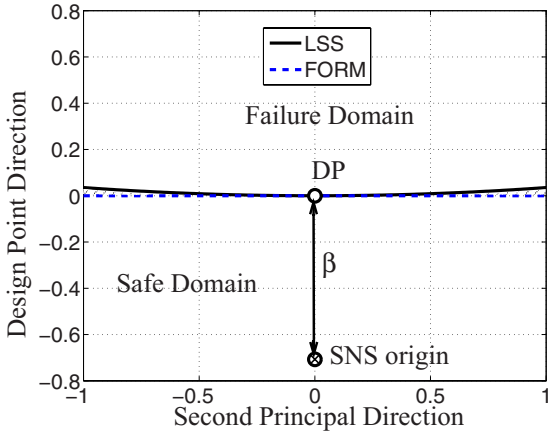

Fig. 3. MVPP for time-invariant reliability analysis with analytical LSF: visualization in the second PP (shaded area=difference between actual failure domain and its FORM approximation)

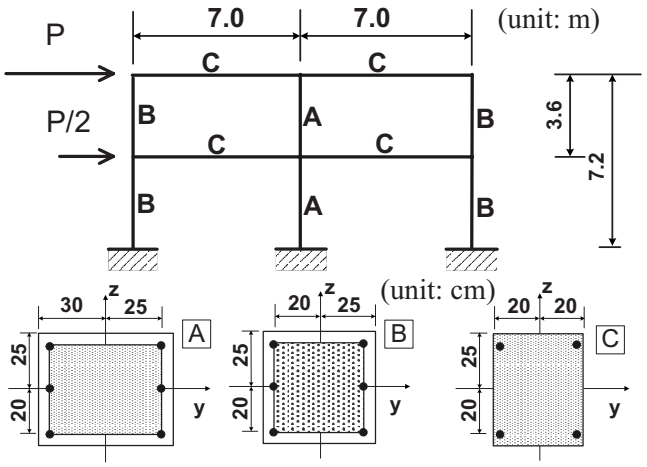

Fig. 4. Geometry, cross-sectional properties, and applied horizontal loads for the two-story RC frame model

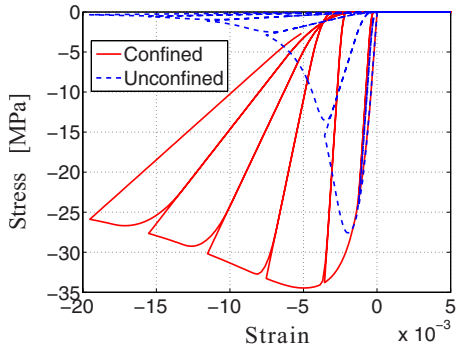

Fig. 5. Material constitutive model for confined and unconfined concrete of the two-story RC frame

tion by FORM of the probability content of the (convex) failure domain in the corresponding PP (e.g., Figs. 2 and 3), while a negative principal curvature yields an underestimation by FORM of the probability content of the (concave) failure domain in the corresponding PP.

Time-Invariant Case: Quasi-Static Pushover of an RC Frame Structure

The second application example considers the two-story two-bay reinforced concrete (RC) frame on rigid foundation represented in Fig. 4. This frame structure is modeled using displacement-based Euler-Bernoulli frame elements with distributed plasticity, each with four Gauss-Legendre integration points along its length. Each beam and column of the frame is discretized into three frame elements for satisfactory accuracy of the computed response. Section stress resultants at the integration points are computed through fiber-section discretization. The constitutive behavior of the reinforcement steel is represented via a uniaxial Menegotto-Pinto constitutive model with linear kinematic hardening (Menegotto and Pinto 1973). The concrete is modeled based on the Popovics-Saenz model with zero tension stiffening for the envelope curve (Kwon and Spacone 2002). The cyclic part of the concrete model is modified from Zona et al. (2004) by smoothing the unloading/reloading branches with third-order polynomials in order to preserve the smoothness of the monotonic envelope in the cyclic behavior. Different material parameters are used for the confined (core) and unconfined (cover) concrete in the columns, while the concrete in the beams is modeled as unconfined. Typical stress-strain cyclic responses of the confined and unconfined concrete materials used in this application example are shown in Fig. 5.

Thirteen material constitutive parameters are used to characterize the various structural materials present in the structure, namely five parameters each for the confined concrete ($f_{c,\text{core}}$ =peak strength; $\varepsilon_{c,\text{core}}$=strain at peak strength; $f_{\text{cu,core}}$=residual strength; $\varepsilon_{\text{cu,core}}$=strain at which the residual strength is reached; $E_{c,\text{core}}$=initial tangent stiffness) and the unconfined (cover) concrete ($f_{c,\text{cover}}$, $\varepsilon_{c,\text{cover}}$, $f_{\text{cu,cover}}$, $\varepsilon_{\text{cu,cover}}$, and $E_{c,\text{cover}}$), and three parameters for the reinforcement steel (f_y=yield strength; E_0 =initial stiffness; and b=postyield to initial stiffness ratio). Each material parameter is modeled with a single random variable over the entire structure. The marginal PDFs of these material parameters are given in Table 1 and are consistent with studies reported in the literature and based on real data (Mirza and MacGregor 1979; Mirza et al. 1979). The statistical correlation coefficients between the various material parameters are chosen based on engineering judgment as follows:

1. $\rho=0.7$:
   a. $f_{c,\text{core}}-f_{\text{cu,core}}$;
   b. $\varepsilon_{c,\text{core}}-\varepsilon_{\text{cu,core}}$;
   c. $\varepsilon_{c,\text{cover}}-\varepsilon_{\text{cu,cover}}$;
   d. $f_{c,\text{core}}-f_{\text{c,cover}}$;
   e. $\varepsilon_{c,\text{core}}-\varepsilon_{c,\text{cover}}$;
   f. $\varepsilon_{\text{cu,core}}-\varepsilon_{\text{cu,cover}}$;
   g. $E_{c,\text{core}}-E_{c,\text{cover}}$,
   h. $f_{c,\text{cover}}-f_{\text{cu,cover}}$;
   i. $f_{\text{cu,core}}-f_{\text{cu,cover}}$.
2. $\rho=0.5$:
   a. $f_{\text{cu,core}}-f_{c,\text{cover}}$;
   b. $\varepsilon_{c,\text{core}}-\varepsilon_{\text{cu,cover}}$;
   c. $\varepsilon_{\text{cu,core}}-\varepsilon_{c,\text{cover}}$;
   d. $f_{c,\text{core}}-f_{\text{cu,cover}}$.
3. $\rho=0.0$ for all other pairs of material constitutive parameters.

After static application of the gravity loads (defined as uniformly distributed load per unit length of beam Q=42.5 kN/m at each floor), the structure is subjected to a quasi-static monotonic pushover analysis, in which an upper triangular distribution of

Table 1. Marginal PDFs, Mean, COV, and DP Values of Basic Random Variables for the Two-Story RC Frame

RV (unit)	Distribution	Mean	COV (%)	DP
$f_{c,\text{core}}$ (MPa)	Lognormal	34.47	20	31.82
$f_{\text{cu,core}}$ (MPa)	Lognormal	25.72	20	24.13
$\varepsilon_{c,\text{core}}$ (—)	Lognormal	0.005	20	0.0049
$\varepsilon_{\text{cu,core}}$ (—)	Lognormal	0.020	20	0.0195
$E_{c,\text{core}}$ (MPa)	Lognormal	27,850	20	24,160
$f_{c,\text{cover}}$ (MPa)	Lognormal	27.58	20	25.10
$f_{\text{cu,cover}}$ (MPa)	Lognormal	1.00	20	0.93
$\varepsilon_{c,\text{cover}}$ (—)	Lognormal	0.002	20	0.0019
$\varepsilon_{\text{cu,cover}}$ (—)	Lognormal	0.012	20	0.0167
$E_{c,\text{cover}}$ (MPa)	Lognormal	24,910	20	26,970
f_y (MPa)	Lognormal	248.20	10.6	232.5
E_0 (MPa)	Lognormal	210,000	3.3	209,700
b (—)	Lognormal	0.02	20	0.0195
P (kN)	Lognormal	350	20	502.9

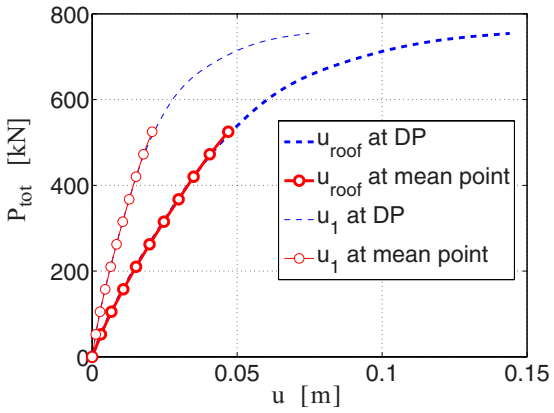

Fig. 6. Base shear-horizontal floor displacements of two-story RC frame structure with basic random variables equal to their mean values (mean point) and to their values at the DP

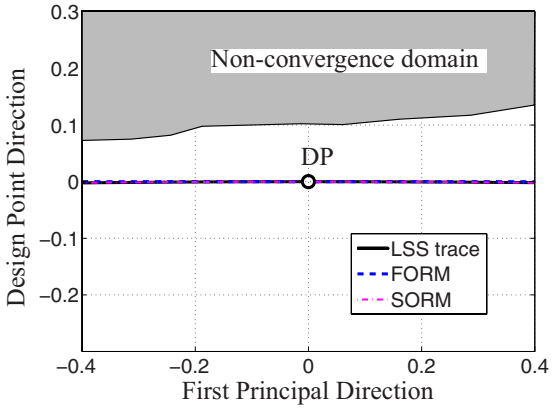

Fig. 7. MVPP for time-invariant reliability analysis of a RC frame structure subjected to quasi-static pushover loads: visualization in the first PP

random horizontal forces is applied at the floor levels (see Fig. 4). The horizontal force applied at the roof level, P, is modeled as a lognormal random variable with mean $\mu_P=350$ kN and COV $=20\%$ (see Table 1), while the horizontal force applied at the second floor level is defined as $P/2$ (i.e., fully correlated with the force applied at the roof level). FE response, response sensitivity and reliability analyses are performed using the FE analysis framework OpenSees, in which the considered material constitutive models were implemented and augmented for response sensitivity analysis (Barbato and Conte 2006; Barbato 2007).

A roof displacement $u_{\text{roof}} \geq u_{\text{lim}}=0.144$ m (corresponding to a roof drift ratio of 2.0% and computed from the horizontal displacement of the top of the middle column) is considered as failure condition. Thus, the LSF is defined as $g=0.144$ m$-u_{\text{roof}}$. The DP search is performed by using the constrained nonlinear optimization software SNOPT and taking the origin of the standard normal space as starting point. Fig. 6 shows the base shear-horizontal floor displacement responses (recorded at the top of the middle column of each story) of the frame structure subjected to quasi-static pushover loads and with random variables set at their mean values and at their DP values (Table 1), respectively. The first-order reliability index obtained is $\beta_{\text{FORM}}=2.048$ and the FORM estimate of the failure probability is $P_{f,\text{FORM}}=0.0203$. After computing all 13 principal curvatures of the LSS at the DP (the first eight of which are reported in Table 2, together with the corresponding $|\beta\kappa_i|$ values), the SORM approximations using Breitung's and Hohenbichler-Rackwitz's formula are obtained as $P_{f,\text{SORM,B}}=0.0209$ and $P_{f,\text{SORM,HR}}=0.0211$, respectively. Monte Carlo simulation (MCS) yields the estimate $P_{f,\text{MCS}}=0.0221$ (from 150,000 samples for COV$[P_{f,\text{MCS}}]=0.017$), which is used as reference solution. It is observed that both FORM and SORM analyses provide sufficiently accurate estimates of the failure probability for this application example. The SORM approximation based on Hohenbichler-Rackwitz's formula is the most accurate of the asymptotic approximations considered here and requires the same computational effort as the SORM approximation based on Breitung's formula. MCS is computationally very expensive (about 2,000 times more expensive than SORM).

Table 2. Principal Curvatures of the LSSs at the DP Used in the MVPP Method for the Application Examples of Time-Invariant and Time-Variant Reliability Analysis

Principal directions	Time-invariant problem ($\beta=2.048$)		Time-variant problem ($t=5$ s) ($\beta=3.409$)	
	Curvature κ_i	$\lvert\beta\kappa_i\rvert$	Curvature κ_i	$\lvert\beta\kappa_i\rvert$
1	−0.0223	0.0457	5.2874	18.0258
2	−0.0138	0.0284	1.1437	3.8990
3	0.0079	0.0161	0.3238	1.1038
4	−0.0054	0.0110	0.0690	0.2351
5	0.0031	0.0063	−0.0121	0.0414
6	−0.0018	0.0037	−0.0107	0.0366
7	0.0015	0.0030	−0.0031	0.0104
8	−0.0014	0.0029	−0.0025	0.0085

The MVPP method is then applied to this example using the results of the reliability analyses performed. In particular, the DP, the principal directions and curvatures are already available (the DP is necessary for FORM and SORM, while the principal directions and curvatures are required by SORM). The values of $|\beta\kappa_i|$ are all very small (see Table 2), and therefore only small differences are expected between the traces of the actual LSS and its first-order approximation. Fig. 7 shows the trace of the actual LSS in the first PP together with the traces of the FORM and SORM approximations of the LSS at the DP. The same figure also indicates the domain in which the FE analyses do not converge (in short: nonconvergence domain). The trace of the LSS in the first PP is obtained through the ZLCM using a grid of points in the considered PP extending from −0.3 to +0.3 in the direction of the DP vector $\boldsymbol{y}^*$ and from −0.4 to +0.4 in the first principal direction. The LSF is evaluated at 41 grid points in each direction of the PP, for a total of $n_{\text{FE}}=41^2-1=1,680$ FE analyses. At the grid point corresponding to the DP, no additional FE analysis is required since LSF$=0$. Determination via the ZLCM of the trace of the LSS in each of the PPs considered is computationally very expensive, but the computed traces can be used as reference solutions for testing more efficient trace finding methods such as the ZFM defined above. The traces of the actual LSS and its first- and second-order approximations at the DP are very close in the first PP. Fig. 8 provides a zoom view of Fig. 7, with the vertical axis magnified by a factor of 200, in which the small differences between the traces of the actual LSS and its first/second-order approximations can be better appreciated. The SORM approximation of the LSS is obtained as the paraboloid tangent to the LSS at the DP with principal curvatures κ_i $(i=1,\ldots,13)$. Fig. 8 also shows the trace of the LSS obtained through the ZFM by using only 58 FE analyses (performed during the line search

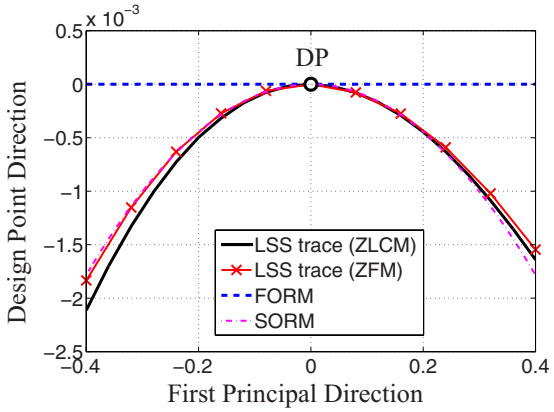

Fig. 8. MVPP for time-invariant reliability analysis of a RC frame structure subjected to quasi-static pushover loads: visualization in the first PP (zoom view)

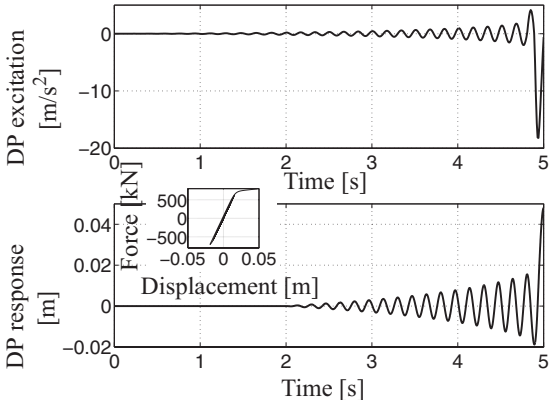

Fig. 9. Design point at time $t=5.0$ s for time-variant reliability analysis of a nonlinear hysteretic SDOF system subjected to white noise base excitation: DP excitation (top), DP roof displacement time history (bottom), and DP base shear-roof displacement response (inset)

along the DP direction for each of 10 discrete values of the abscissa along the principal direction). The trace obtained by means of the ZFM is very close to that computed using the ZLCM. In this example, the nonconvergence domain significantly overlaps with the failure domain as seen in Fig. 7. Nonconvergence domains are common in FE reliability analysis based on nonlinear hysteretic structural models with degrading behavior, such as the RC frame model considered here. The existence of a nonconvergence domain requires appropriate handling of the non-converged sample points to obtain a reliable failure probability estimate using simulation methods. In this paper, the MCS result is obtained by repeating the FE analysis for all samples of the random model parameters corresponding to non-convergence cases. These new FE analyses are performed by using smaller load increments and a displacement-control solution strategy in order to compute the LSF values. This procedure is feasible for the problem considered here due to its relatively small size. For more complex large-scale real-world applications, a more general and efficient approach is needed, the development of which is outside the scope of this paper. The visualization of the LSS using the MVPP method explains the good agreement between the FORM, SORM and MCS results obtained for this problem. The negative first and second eigenvalues of the Hessian matrix of the LSF at the DP (or principal curvatures of the LSS at the DP) suggest that, in this example, FORM underestimates the failure probability, which is confirmed by the MCS result.

Time-Variant Case: Nonlinear Hysteretic SDOF System Subjected to White Noise Excitation

In a third application example, the MVPP method is applied to the time-variant reliability analysis of a nonlinear hysteretic single-degree-of-freedom (SDOF) system subjected to Gaussian white noise base excitation. The base excitation process is discretized into Gaussian random variables representing the value of the ground acceleration at discrete times with a constant time interval $\Delta t=0.01$ s. The ground acceleration process is then linearly interpolated inside each of the time intervals. The SDOF system is characterized by a force-deformation relation modeled using the Menegotto-Pinto constitutive law. This constitutive law is calibrated to a shear-type single-story steel frame with height $H=3.20$ m, bay length $L=6.00$ m and made of European HE340A wide flange steel beams. The system is defined by the following parameters (taken as deterministic): mass $M=28,800$ kg, damping ratio $\zeta=0.02$, initial stiffness $K=40.56$ kN/mm, initial yield force $F_{y0}=734$ kN, and post-yield to initial stiffness ratio $b=0.05$.

Fig. 9 plots the DP excitation (top), the DP roof displacement time history (bottom), and the DP base shear-roof displacement response (inset) for a failure event occurring at time $t=5.0$ s, with failure defined as the roof displacement exceeding the threshold $\xi=0.048$ m (single-barrier up-crossing problem, Lutes and Sarkani 2004), corresponding to a roof drift ratio of 1.5%. Both DP excitation and DP roof displacement time histories are characterized by low values for most of their duration and very high values at their ends. These time history profiles at the DP are significantly different from their counterparts for the linear elastic case, in which the DP excitation and the DP roof displacement values increase gradually with time (Drenick 1970). The SDOF system behaves almost linearly for $t<4.9$ s, and strongly nonlinearly for $t\geq 4.9$ s. This DP behavior is typical of the first-yield excursion condition of structural systems modeled using the Menegotto-Pinto constitutive model and subjected to white noise excitation (Conte et al. 2008).

Table 2 reports the first eight principal curvatures and the corresponding $|\beta\kappa_i|$ values for the LSS corresponding to a failure event occurring at time $t=5.0$ s. It is observed that: (1) the first three principal curvatures are relatively very large in magnitude compared to the remaining ones; (2) the magnitude of the principal curvatures (sorted from highest to lowest absolute value) decreases very fast with their order; and (3) even if the number of random variables (i.e., the random values of the ground acceleration at all discrete times) is quite large ($n=500$) in this problem, only a few PPs are needed to visualize the nonlinear behavior of the LSS in the neighborhood of the DP. In this specific case, setting $|\beta\kappa|_{\min}=0.5$, the MVPP method requires to visualize the LSS using FE analysis in only three PPs. Figs. 10–12 show the MVPP-based visualization, in the first three PPs, of the two LSSs ($G_1=0$ and $G_2=0$) employed in the computation of the MOCR at time $t=5.0$ s using $\delta t=0.005$ s in Eq. (6). Also in this case, the ZFM (requiring 285 simulations over the first three PPs combined) is much more efficient than the ZLCM (requiring 1,323 simulations), while the two methods provide practically coincident results. From these three figures, it is observed that: (1) the difference between the traces of the actual LSSs at times 5.0 s ($G_1=0$) and 5.005 s ($G_2=0$) and the traces of their FORM ap-

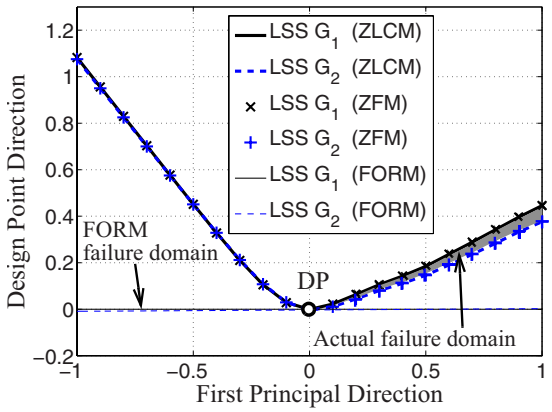

Fig. 10. MVPP for time-variant reliability analysis of a nonlinear hysteretic SDOF system subjected to white noise base excitation (t =5 s, δt=0.005 s): visualization in the first PP

proximations is very significant; and (2) the failure domain obtained using the FORM approximations of the LSSs differs significantly from the actual failure domain needed in the numerator on the r.h.s. of Eq. (6) for MOCR computation.

Fig. 13 compares the expected cumulative number of up-crossing events, $E[N(t)]$, and the time-variant failure probability,

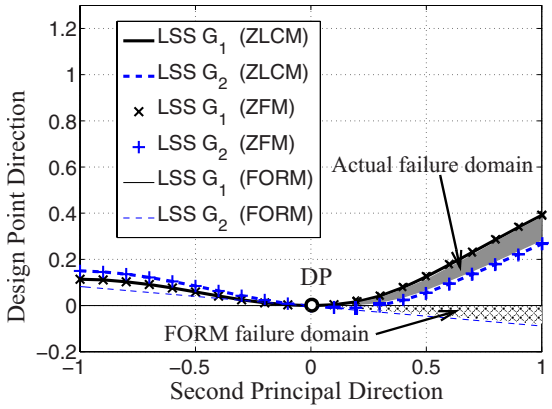

Fig. 11. MVPP for time-variant reliability analysis of a nonlinear hysteretic SDOF system subjected to white noise base excitation (t =5 s, δt=0.005 s): visualization in the second PP

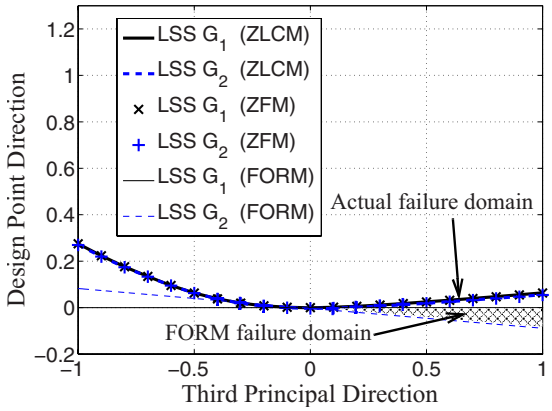

Fig. 12. MVPP for time-variant reliability analysis of a nonlinear hysteretic SDOF system subjected to white noise base excitation (t =5 s, δt=0.005 s): visualization in the third PP

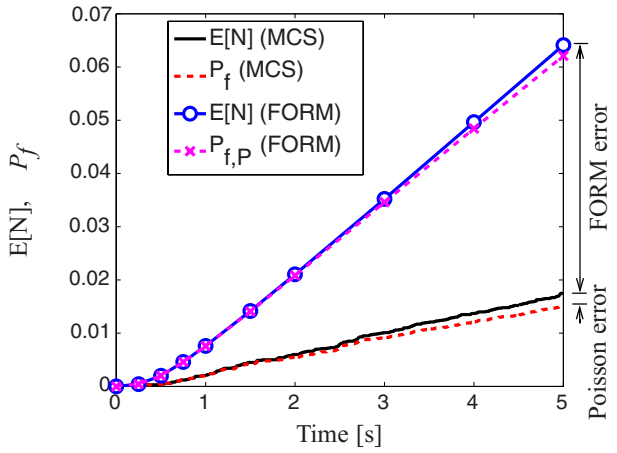

Fig. 13. Time-variant reliability analysis of a nonlinear hysteretic SDOF system subjected to white noise base excitation: estimates of expected cumulative number of up-crossings, E[N], and time-variant failure probability, P_f, using MCS and FORM-based MOCR computation

$P_f(t)$, estimated using MCS and FORM-based MOCR computation for $0 \ s \leq t \leq 5 \ s$. It is observed that the Poisson approximation of the failure probability, $P_{f,P}(t)$ (Lutes and Sarkani 2004), based on FORM-based MOCR computation (in short, FORM-based Poisson approximation) provides remarkably inaccurate results compared to MCS. The FORM-based Poisson approximation suffers from two sources of error: (1) inaccuracy of the hypothesis of statistical independence of up-crossing events, which is the basis of the Poisson approximation; and (2) inaccuracy of the FORM approximations at the DP of the two nonlinear LSSs used to compute the MOCR at a given instant of time. For this application example, the results shown in Fig. 13 indicate that the inaccuracy of the FORM-based Poisson approximation is due principally to the inaccuracy of the FORM approximations due to a pronounced nonlinearity of the LSSs at their DPs. The MVPP results presented in Figs. 10–12 confirm this expected strong nonlinearity of the LSSs at their DPs in the first three PPs.

Conclusions

In the context of FE reliability analysis, this paper introduces a new method, referred to as the MVPP method, to visualize LSSs near their design points DPs in high-dimensional spaces. This method consists of visualizing the traces of the LSS in the neighborhood of a DP in planes of particular interest, referred to as PPs. The PPs are defined as the planes of principal curvatures of the LSS at the DP, in decreasing order of magnitude of the principal curvatures.

The MVPP method provides very useful information about the topology of the LSS, identifying a small number of PPs in which the traces of the LSS are significantly nonlinear, and thus requiring only a limited number of FE analyses (i.e., proportional to the number of identified PPs). For the application examples of time-invariant and time-variant reliability analysis presented in this paper, the visualization results obtained using the MVPP method are used to investigate the sources of error of the failure probability estimates provided by FORM/SORM as compared to the

"exact" failure probability determined through Monte Carlo simulation and importance sampling.

The newly gained insight into the topology of the LSS at the DP is being used by the writers to develop more efficient and more accurate computational reliability methods for evaluating the probability content of failure domains typically encountered in FE reliability analysis.

Acknowledgments

The writers gratefully acknowledge support of this research by (1) the National Science Foundation under Grant No. CMS-0010112, (2) the Pacific Earthquake Engineering Research Center (PEER) Center's Transportation Systems Research Program under under Award No. 00006493, and (3) the Louisiana Board of Regents through the Pilot Funding for New Research Program of the National Science Foundation Experimental Program to Stimulate Competitive Research under Award No. NSF(2008)-PFUND-86. Any opinions, findings, conclusions or recommendations expressed in this publication are those of the writers and do not necessarily reflect the views of the sponsors.

References

Ang, G. L., Ang, A. H.-S., and Tang, W. H. (1992). "Optimal importance sampling density estimator." *J. Eng. Mech.*, 118(6), 1146–1163.

Au, S. K., and Beck, J. L. (2001a). "Estimation of small failure probabilities in high dimensions by subset simulation." *Probab. Eng. Mech.*, 16(4), 263–277.

Au, S. K., and Beck, J. L. (2001b). "First excursion probabilities for linear systems by very efficient importance sampling." *Probab. Eng. Mech.*, 16(3), 193–207.

Au, S. K., and Beck, J. L. (2003). "Subset simulation and its application to seismic risk based on dynamic analysis." *J. Eng. Mech.*, 129(8), 901–917.

Au, S. K., Papadimitriou, C., and Beck, J. L. (1999). "Reliability of uncertain dynamical systems with multiple design points." *Struct. Safety*, 21(2), 113–133.

Barbato, M. (2007). "Finite element response sensitivity, probabilistic response and reliability analyses of structural systems with applications to earthquake engineering." Ph.D. thesis, Univ. of California at San Diego, La Jolla, Calif.

Barbato, M., and Conte, J. P. (2005). "Finite element response sensitivity analysis: A comparison between force-based and displacement-based frame element models." *Comput. Methods Appl. Mech. Eng.*, 194, (12–16), 1479–1512.

Barbato, M., and Conte, J. P. (2006). "Finite element structural response sensitivity and reliability analyses using smooth versus non-smooth material constitutive models." *Int. J. Reliab.*, 1(1/2), 3–39.

Barbato, M., Zona, A., and Conte, J. P. (2007). "Finite element response sensitivity analysis using three-field mixed formulation: General theory and application to frame structures." *Int. J. Numer. Methods Eng.*, 69(1), 114–161.

Breitung, K. (1984). "Asymptotic approximations for multinormal integrals." *J. Engrg. Mech. Div.*, 110(3), 357–366.

Bucher, C. G. (1988). "Adaptive importance sampling—An iterative fast Monte Carlo procedure." *Struct. Safety*, 5(2), 119–126.

Conte, J. P., Barbato, M., and Gu, Q. (2008). "Finite element response sensitivity, probabilistic response and reliability analyses." Chap. 2, *Computational structural dynamics and earthquake engineering*, Vol. 2, M. Papadrakakis, D. C. Champis, Y. Tsompanakis, N. D. Lagaros, eds., Structures & Infrastructures Series, Taylor & Francis, London.

Conte, J. P., Barbato, M., and Spacone, E. (2004). "Finite element response sensitivity analysis using force-based frame models." *Int. J. Numer. Methods Eng.*, 59(13), 1781–1820.

Conte, J. P., Vijalapura, P. K., and Meghella, M. (2003). "Consistent finite-element response sensitivity analysis." *J. Eng. Mech.*, 129, 1380–1393.

Der Kiureghian, A. (2000). "The geometry of random vibrations and solutions by FORM and SORM." *Probab. Eng. Mech.*, 15(1), 81–90.

Der Kiureghian, A., and De Stefano, M. (1991). "Efficient algorithms for second-order reliability analysis." *J. Eng. Mech.*, 117(12), 2904–2923.

Der Kiureghian, A., and Ke, J.-B. (1988). "The stochastic finite element method in structural reliability." *Probab. Eng. Mech.*, 3(2), 83–91.

Der Kiureghian, A., Lin, H.-Z., and Hwang, S.-J. (1987). "Second-order reliability approximations." *J. Engrg. Mech. Div.*, 113(EM8), 1208–1225.

Ditlevsen, O., and Madsen, H. O. (1996). *Structural reliability methods*, Wiley, New York.

Drenick, R. F. (1970). "Model-free design of aseismic structures." *J. Engrg. Mech. Div.*, 96(EM4), 483–493.

Filippou, F. C., and Constantinides, M. (2004). "FEDEASLab getting started guide and simulation examples." *Rep. No. NEESgrid-2004-22*, NEESgrid SI, Davis, Calif., ⟨http://fedeaslab. berkeley.edu/⟩ (Aug. 2010).

Gill, P. E., Murray, W., and Saunders, M. A. (2002). "SNOPT: An SQP algorithm for large-scale constrained optimization." *SIAM J. Optim.*, 12, 979–1006.

Gill, P. E., Murray, W., and Wright, M. H. (1981). *Practical optimization*, Academic, New York.

Gu, Q. (2008). "Finite element response sensitivity and reliability analysis of soil-foundation-structure-interaction (SFSI) systems." Ph.D. thesis, Univ. of California at San Diego, La Jolla, Calif.

Gu, Q., Barbato, M., and Conte, J. P. (2009a). "Handling of constraints in finite element response sensitivity analysis." *J. Eng. Mech.*, 135(12), 1427–1438.

Gu, Q., Conte, J. P., Elgamal, A., and Yang, Z. (2009b). "Finite element response sensitivity analysis of multi-yield-surface J_2 plasticity model by direct differentiation method." *Comput. Methods Appl. Mech. Eng.*, 198(30–32), 2272–2285.

Hagen, O., and Tvedt, L. (1991). "Vector process out-crossing as parallel system sensitivity measure." *J. Eng. Mech.*, 117(10), 2201–2220.

Haukaas, T. (2001). "FERUM (finite element reliability using Matlab)." *User's Guide*, ⟨http://www.ce.berkeley.edu/projects/ferum⟩ (Aug. 2010).

Haukaas, T., and Der Kiureghian, A. (2004). "Finite element reliability and sensitivity methods for performance-based engineering." *Pacific Earthquake Engineering Research Center Rep. No. PEER 2003/14*, Univ. of California, Berkeley, Calif.

Hohenbichler, M., and Rackwitz, R. (1986). "Sensitivity and importance measures in structural reliability." *Civ. Eng. Syst.*, 3(4), 203–209.

Hohenbichler, M., and Rackwitz, R. (1988). "Improvement of second-order reliability estimates by importance sampling." *J. Engrg. Mech. Div.*, 114(12), 2195–2199.

Kleiber, M., Antunez, H., Hien, T. D., and Kowalczyk, P. (1997). *Parameter sensitivity in nonlinear mechanics: Theory and finite element computation*, Wiley, New York.

Kwon, M., and Spacone, E. (2002). "Three-dimensional finite element analyses of reinforced concrete columns." *Comput. Struct.*, 80, 199–212.

Liu, P.-L., and Der Kiureghian, A. (1991). "Optimization algorithms for structural reliability." *Struct. Safety*, 9(3), 161–177.

Lutes, L. D., and Sarkani, S. (2004). *Random vibrations*, Elsevier, Burlington, Mass.

MathWorks. (1997). "Matlab—High performance numeric computation and visualization software." *User's guide*, Natick, Mass.

Mazzoni, S., McKenna, F., Scott M. H., and Fenves, G. L. (2007). *OpenSees command language manual*, Pacific Earthquake Engineering Center, Univ. of California, Berkeley, Berkeley, Calif., ⟨http://opensees.berkeley.edu/OpenSees/manuals/usermanual/OpenSeesCommandLanguageManual.pdf⟩ (Aug. 2010).

Melchers, R. E. (1989). "Importance sampling in structural systems." *Struct. Safety*, 6(1), 3–10.
Menegotto, M., and Pinto, P. E. (1973). "Method for analysis of cyclically loaded reinforced concrete plane frames including changes in geometry and non-elastic behavior of elements under combined normal force and bending." *Proc., IABSE Symp. on "Resistance and Ultimate Deformability of Structures Acted on by Well-Defined Repeated Loads"*, IABSE, Zurich, Switzerland.
Mirza, S. A., and MacGregor, J. G. (1979). "Variability of mechanical properties of reinforcing bars." *J. Struct. Div.*, 105(5), 921–937.
Mirza, S. A., MacGregor, J. G., and Hatzinikolas, M. (1979). "Statistical descriptions of strength of concrete." *J. Struct. Div.*, 105(6), 1021–1037.
Schueller, G. I. (2008). "Computational stochastic dynamics—Some lessons learned." *Computational structural dynamics and earthquake engineering*, M. Papadrakakis, D. C. Charmpis, D. Nikos, N. D. Lagaros, and Y. Tsompanakis, eds., Taylor & Francis, London, 3–20.
Schueller, G. I., Pradlwarter, H. J., and Koutsourelakis, P. S. (2004). "A critical appraisal of reliability estimation procedures for high dimensions." *Probab. Eng. Mech.*, 19(4), 463–474.
Stoer, J., and Bulirsch, R. (2002). *Introduction to numerical analysis*, 3rd Ed., Springer, Berlin.
Zhang, Y., and Der Kiureghian, A. (1993). "Dynamic response sensitivity of inelastic structures." *Comput. Methods Appl. Mech. Eng.*, 108(1–2), 23–36.
Zona, A., Barbato, M., and Conte, J. P. (2004). "Finite element response sensitivity analysis of steel-concrete composite structures." *Rep. No. SSRP-04/02*, Dept. of Structural Engineering, Univ. of California at San Diego, La Jolla, Calif.
Zona, A., Barbato, M., and Conte, J. P. (2005). "Finite element response sensitivity analysis of steel-concrete composite beams with deformable shear connection." *J. Eng. Mech.*, 131(11), 1126–1139.
Zona, A., Barbato, M., and Conte, J. P. (2006). "Finite element response sensitivity analysis of continuous steel-concrete composite girders." *Steel Compos. Struct.*, 6(3), 183–202.